Communication

A Theoretical Investigation of the Structural, Electronic and Mechanical Properties of Pristine and Nitrogen-Terminated Carbon Nanoribbons Composed of 4–5–6–8-Membered Rings

Bohayra Mortazavi

Department of Mathematics and Physics, Leibniz Universität Hannover, Appelstraße 11,
30167 Hannover, Germany; bohayra.mortazavi@gmail.com

Abstract: Among the exciting recent advances in the field of carbon-based nanomaterials, the successful realization of a carbon nanoribbon composed of 4–5–6–8-membered rings (ACS Nano 2023 17, 8717) is a particularly inspiring accomplishment. In this communication motivated by the aforementioned achievement, we performed density functional theory calculations to explore the structural, electronic and mechanical properties of the pristine 4–5–6–8-membered carbon nanoribbons. Moreover, we also constructed four different nitrogen-terminated nanoribbons and analyzed their resulting physical properties. The acquired results confirm that the pristine and nitrogen-terminated nanoribbons are are thermally stable direct-gap semiconductors, with very close HSE06 band gaps between 1.12 and 1.25 eV. The elastic modulus and tensile strength of the nitrogen-free 4–5–6–8-membered nanoribbon are estimated to be remarkably high, 534 and 41 GPa, respectively. It is shown that nitrogen termination can result in noticeable declines in the tensile strength and elastic modulus to 473 and 33 GPa, respectively. This study provides useful information on the structural, thermal stability, electronic and mechanical properties of the pristine and nitrogen-terminated 4–5–6–8-membered carbon nanoribbons and suggests them as strong direct-gap semiconductors for electronics, optoelectronics and energy storage systems.

Keywords: carbon nanoribbons; density functional theory; semiconductor; mechanical

1. Introduction

Carbon, owing to its exceptional physics and chemistry, can appear in a wide range of allotropes, spanning from zero to three-dimensional lattices, including zero-dimensional fullerenes [1] and carbyne, one-dimensional (1D) carbon nanotubes, two-dimensional (2D) graphene [2–4], graphyne and graphdiyne [5] and three-dimensional graphite and diamond. Over time, different carbon allotropes have been discovered, each displaying fascinating properties with potential applications in numerous fields. Among various carbon structures, graphene [2–4], the so-called wonder material, has received significant attention due to its unique electronic, mechanical, thermal and optical characteristics. However, the lack of a finite electronic bandgap restricts the usefulness of graphene nanosheets in electronic and optoelectronic nanodevices. One effective approach to adjusting the bandgap of graphene involves modifying its topology and altering the original hexagonal rings with tetragonal, pentagonal, heptagonal and octagonal rings. Theoretical calculations have confirmed that 2D carbon structures with non-hexagonal carbon rings can show diverse electronic properties, from metallic to semimetallic and semiconducting behaviors [6–15]. Nonetheless, due to being metastable, the experimental realization of large-area planar carbon lattices with non-hexagonal rings is challenging and consequently involves employing chemical reaction processes. In an outstanding recent breakthrough by Fan et al. [6], a two-step polymerization method was devised utilizing a gold catalyst which could successfully produce a biphenylene 2D network, a full-carbon lattice made entirely from 4–6–8-membered rings.

In the latest advancement, Kang and coworkers [16] carried out face-to-face dehydrogenative reactions of polyfluorene chains, triggering on-surface lateral fusion, and subsequently realized for the first time a carbon nanoribbon composed of 4–5–6–8-membered rings which shows a semiconducting electronic bandgap of ~1.4 eV. In recent years, 2D lattices consisting of covalently bonded carbon and nitrogen atoms have attracted remarkable attention because of their exceptional physics and chemistry. Among them, several lattices have been successfully realized, such as s- and tri-triazine-based graphitic carbon nitride g-C_3N_4 [17], nanoporous C_2N [18], all-triazine C_3N_3 [19], polyaniline-based C_3N [20], and s-heptazine C_3N_5 [21], which all show semiconducting electronic natures. Taking into account the exceptional ability of nitrogen and carbon atoms to form strong covalent interactions, there exists also the possibility of realizing nitrogen-terminated 4–5–6–8-membered carbon nanoribbons. In particular, it is already well known that nitrogen-doped carbon-based structures can show superior performances in energy storage applications [22]. On this basis, inspired by the latest experimental achievement by Kang et al. [16], we performed density functional theory (DFT) calculations to explore the structural, thermal stability, electronic and mechanical properties of the pristine and nitrogen-terminated 4–5–6–8-membered carbon nanoribbons [23–29]. The theoretical results confirm the remarkably high elastic moduli, tensile strengths and direct-gap semiconducting natures of these novel carbon-based 1D systems, which are highly attractive for further theoretical and experimental endeavors.

2. Computational Methods

The Vienna ab initio simulation package (VASP) [30,31] was used to perform the DFT calculations via employing the Perdew–Burke–Ernzerhof (PBE) and generalized gradient approximation (GGA) methods along with Grimme's DFT-D3 [32] van der Waals (vdW) dispersion correction and a kinetic energy cutoff of 500 eV. Optimizations of both the lattice parameters and atomic positions were conducted via the conjugate gradient method, using a $3 \times 1 \times 1$ Monkhorst–Pack [33] k-point grid with energy and force convergence criteria of 10^{-5} eV and 0.01 eV/Å, respectively. To prevent vdW interactions along the nanoribbons' thicknesses and widths, we adopted 16 and 25 Å sizes along the corresponding directions of the 3D periodic cells. Since the ordinary PBE/GGA tends to underestimate the electronic gap, the HSE06 [34] hybrid functional was employed to acquire more accurate predictions.

3. Results and Discussions

We first investigate the structural characteristics of the pristine and nitrogen-terminated 4–5–6–8-membered carbon nanoribbons, which are illustrated in Figure 1. Figure 1a shows the atomic structure of the pristine C_{52} ($C_{52}H_{16}$) lattice in which the CH groups on the boundary can be replaced with various atoms like N and O and form different synthesizable configurations. In this work, we replaced the 4, 8, and 12 CH groups with nitrogen atoms in order to explore the nitrogen termination effects. It is worth noting that in order to avoid the formation of N-N bonds, we did not consider the replacement of all CH groups in these systems. For the case of termination with four nitrogen atoms, we considered two different configurations: $C_{48}N_4$-1 and $C_{48}N_4$-2. According to our energy minimization results, the sizes of the unitcells along the longitudinal direction for the C_{52}, $C_{48}N_4$-1, $C_{48}N_4$-2, $C_{44}N_8$, and $C_{40}N_{12}$ are predicted to be 16.391, 16.193, 16.225, 16.014, and 15.919 Å, respectively. It is clear that by increasing the content of nitrogen atoms, the structures shrink slightly. From basic physics, it is known that the regions with the weakest bonding can dominate the transport properties. In these systems, two symmetrical C-C bonds in the center of the large interior nanopore clearly play critical roles in the transport properties. The lengths of these critical bonds for the C_{52}, $C_{48}N_4$-1, $C_{48}N_4$-2, $C_{44}N_8$, and $C_{40}N_{12}$ are measured to be 1.484, 1.494, 1.483, 1.491, and 1.482 Å, respectively. For the convenience of oncoming studies, geometry-optimized lattices are included in the Supplementary Materials.
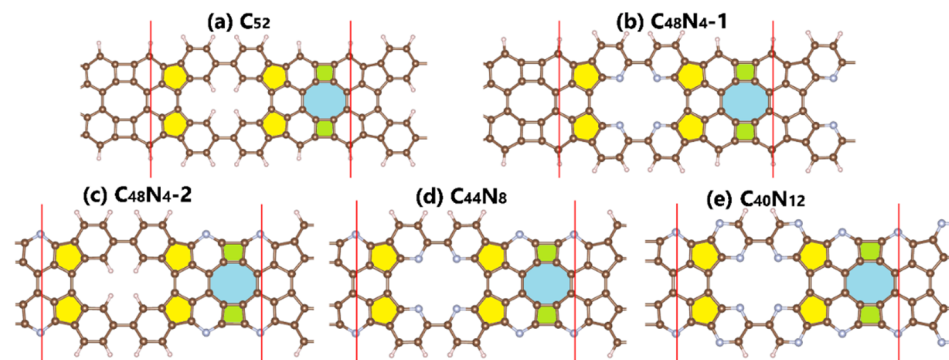
Figure 1. Top views for the atomic structures of the C_{52} (**a**), $C_{48}N_4$-1 (**b**), $C_{48}N_4$-2 (**c**), $C_{44}N_8$ (**d**), and $C_{40}N_{12}$ (**e**) nanoribbons. The green, yellow, and blue colors highlight the 4-, 5-, and 8-membered rings, respectively.

To examine the thermal stability of the C_{52}, $C_{48}N_4$-1, $C_{44}N_8$, and $C_{40}N_{12}$ lattices, we conducted ab initio molecular dynamics (AIMD) simulations at 1000 K with a time step of 1 fs for around 9000 time steps, using a $2 \times 1 \times 1$ K-point grid. The results for the evolution of the systems' total energies, shown in Figure 2, reveal complete structural and energetic stability and consequently confirm that these systems exhibit robust flexibility and could stay completely intact at a relatively high temperature, demonstrating their remarkable thermal stability.
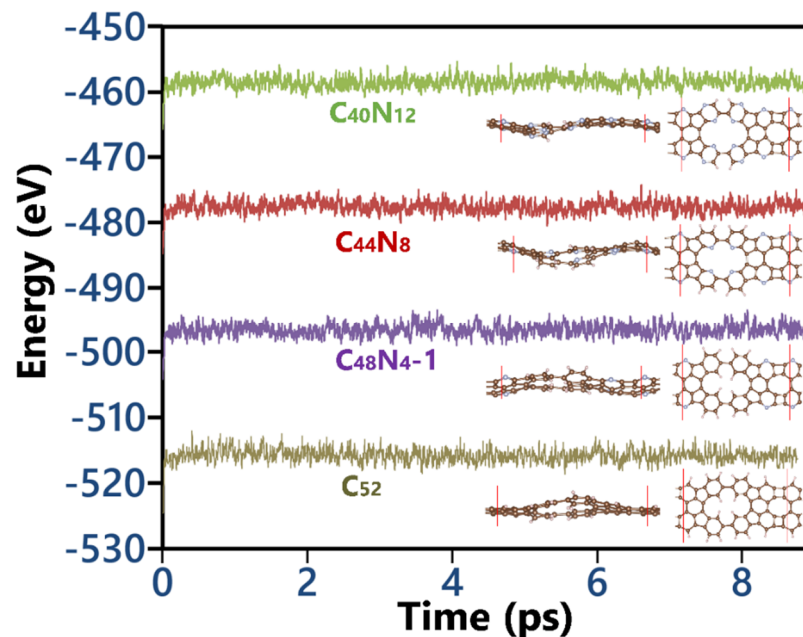

Figure 2. Fluctuations in the total energy during the AIMD simulations at 1000 K. Insets show the top and side views of the final atomic configurations at the end of the AIMD simulations.

Having analyzed the structural characteristics of the pristine and nitrogen-terminated 4–5–6–8-membered carbon nanoribbons, we now shift our attention to the analysis of their electronic features. The electronic band structures of the considered systems are illustrated in Figure 3 on the basis of the PBE/GGA and HSE06 methods. As an interesting preliminary finding with both functionals, all studied systems show direct-gap semiconducting natures occurring at the Γ point. The PBE(HSE06) electronic band gap of the C_{52}, $C_{48}N_4$-1, $C_{48}N_4$-2, $C_{44}N_8$, and $C_{40}N_{12}$ are predicted to be 0.59 (1.12), 0.59 (1.12), 0.65 (1.18), 0.64 (1.19), and 0.69 (1.25) eV, respectively. It is clear that the incorporation of nitrogen atoms into these lattices shows marginal effects in the widening of the band gap. The estimated band gap of 1.12 eV for the C_{52} system is nonetheless shorter than the value of 1.4 eV [16]

that was measured experimentally, which can be either attributed to the substrate effects or the necessity of considering excitonic effects using the advanced GW [35] functional in the calculations.
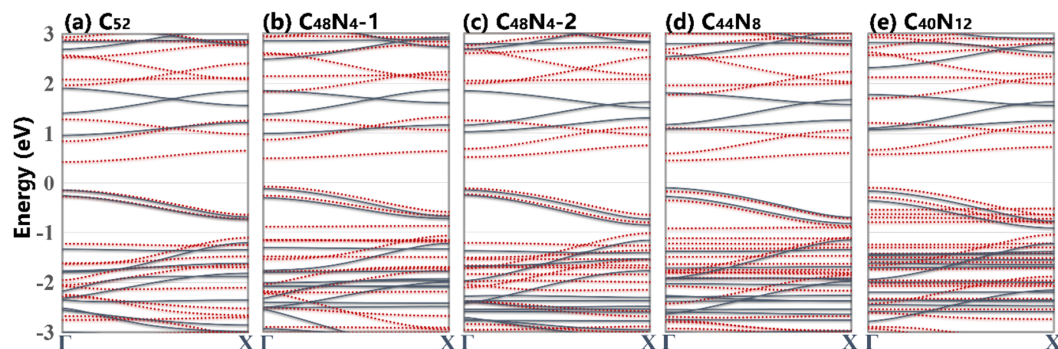

Figure 3. Electronic band structures of the C_{52} (**a**), $C_{48}N_4$–1 (**b**), $C_{48}N_4$–2 (**c**), $C_{44}N_8$ (**d**), and $C_{40}N_{12}$ (**e**) nanoribbons via the the HSE06 (solid dark lines) and PBE/GGA (dotted red lines) methods. The Fermi energy is set at zero.

Last but not least, we now investigate the mechanical properties of the pristine and nitrogen-terminated 4–5–6–8-membered carbon nanoribbons, which could be also examined using the machine learning interatomic potentials [36–40]. In order to report the mechanical properties in the illustrative GPa unit, we assumed the fixed thickness and width of 3.35 and 11.75 Å, respectively, for these nanoribbons according to the vdW dimeter of carbon atoms. According to the stress–strain curves shown in Figure 4, the tensile strengths of the C_{52}, $C_{48}N_4$-1, $C_{48}N_4$-2, $C_{44}N_8$, and $C_{40}N_{12}$ are predicted to be 40.8, 33.3, 40.8, 33.5, and 34.3 GPa, respectively. It is very interesting that the tensile strengths of the C_{52} and $C_{48}N_4$-2 and the $C_{48}N_4$-1$C_{44}N_8$ and $C_{40}N_{12}$ are very close, clearly revealing that the tensile strengths of these 1D systems do not show strong dependencies on the content of nitrogen atoms but on the location of nitrogen termination. As expected, and as also realized from the structural data in Figure 4, the ruptures in these lattices always occur between the two symmetrical C-C bonds in the center of the large interior nanopore. It was found that when the carbon atoms are bonded with a single nitrogen atom, as in the $C_{48}N_4$-1 and $C_{44}N_8$ lattices, the connecting C-C bonds show larger lengths, which naturally induces a weakening effect. It can be concluded that if one of the carbon atoms in the aforementioned bonds is connected with nitrogen atoms, the tensile strength drops from around 41 to 33 GPa; otherwise, the tensile strength is not noticeably affected. The elastic moduli of the C_{52}, $C_{48}N_4$-1, $C_{48}N_4$-2, $C_{44}N_8$, and $C_{40}N_{12}$ systems are predicted to be 534, 500, 510, 473, and 493 GPa, respectively. It is clear that the elastic values are close for different contents of nitrogen atoms, and a clear trend cannot be established. The presented DFT results clearly show the remarkably high mechanical properties of these novel carbon-based 1D systems.
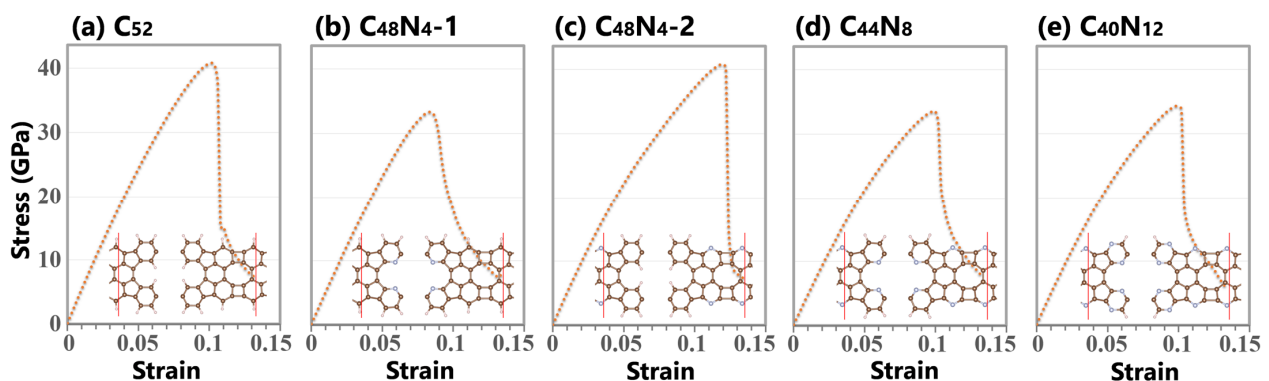

Figure 4. Stress–strain curves of the C_{52} (**a**), $C_{48}N_4$-1 (**b**), $C_{48}N_4$-2 (**c**), $C_{44}N_8$ (**d**), and $C_{40}N_{12}$ (**e**) nanoribbons. Insets show the atomic structures at the strain level around 0.13.

4. Concluding Remarks

In this communication, density functional theory calculations were performed to explore the structural, thermal stability, electronic and mechanical properties of the pristine and nitrogen terminated 4–5–6–8-membered carbon nanoribbons. Molecular dynamics results confirm outstanding thermal stability of the considered nanoribbons. It was confirmed that the pristine and nitrogen-terminated nanoribbons are direct-gap semiconductors at the Γ point, with very close HSE06 band gaps between 1.12 and 1.25 eV. It is shown that the two symmetrical C-C bonds in the center of the large interior nanopore dominate the mechanical strength in these systems. It is found that if one of the carbon atoms in the aforementioned bonds is connected with nitrogen atoms, the tensile strength becomes around 33 GPa; otherwise, it remains around 40 GPa, close to that of the pristine lattice. The elastic modulus was found to vary between 534 and 473 GPa, depending on the location of the nitrogen atoms' termination. The DFT results confirm the outstanding thermal stability and mechanical properties and the highly appealing electronic features of these novel 4–5–6–8-membered carbon-based nanoribbons, motivating more elaborate investigations.

References

1. Ge, M.; Sattler, K. Observation of fullerene cones. *Chem. Phys. Lett.* **1994**, *220*, 192–196. [CrossRef]
2. Novoselov, K.S.; Geim, A.K.; Morozov, S.V.; Jiang, D.; Zhang, Y.; Dubonos, S.V.; Grigorieva, I.V.; Firsov, A.A. Electric field effect in atomically thin carbon films. *Science* **2004**, *306*, 666–669. [CrossRef]
3. Geim, A.K.; Novoselov, K.S. The rise of graphene. *Nat. Mater.* **2007**, *6*, 183–191. [CrossRef] [PubMed]
4. Castro Neto, A.H.; Guinea, F.; Peres, N.M.R.; Novoselov, K.S.; Geim, A.K. The electronic properties of graphene. *Rev. Mod. Phys.* **2009**, *81*, 109–162. [CrossRef]
5. Li, G.; Li, Y.; Liu, H.; Guo, Y.; Li, Y.; Zhu, D. Architecture of graphdiyne nanoscale films. *Chem. Commun.* **2010**, *46*, 3256–3258. [CrossRef]
6. Fan, Q.; Yan, L.; Tripp, M.W.; Krejčí, O.; Dimosthenous, S.; Kachel, S.R.; Chen, M.; Foster, A.S.; Koert, U.; Liljeroth, P.; et al. Biphenylene network: A nonbenzenoid carbon allotrope. *Science* **2021**, *372*, 852–856. [CrossRef] [PubMed]
7. Brunetto, G.; Autreto, P.A.S.; Machado, L.D.; Santos, B.I.; dos Santos, R.P.B.; Galvão, D.S. Nonzero Gap Two-Dimensional Carbon Allotrope from Porous Graphene. *J. Phys. Chem. C* **2012**, *116*, 12810–12813. [CrossRef]
8. Wang, X.-Q.; Li, H.-D.; Wang, J.-T. Prediction of a new two-dimensional metallic carbon allotrope. *Phys. Chem. Chem. Phys.* **2013**, *15*, 2024–2030. [CrossRef] [PubMed]
9. Wang, Z.; Zhou, X.-F.; Zhang, X.; Zhu, Q.; Dong, H.; Zhao, M.; Oganov, A.R. Phagraphene: A Low-Energy Graphene Allotrope Composed of 5–6–7 Carbon Rings with Distorted Dirac Cones. *Nano Lett.* **2015**, *15*, 6182–6186. [CrossRef]
10. Zhang, S.; Zhou, J.; Wang, Q.; Chen, X.; Kawazoe, Y.; Jena, P. Penta-graphene: A new carbon allotrope. *Proc. Natl. Acad. Sci. USA* **2015**, *112*, 2372–2377. [CrossRef]
11. Mortazavi, B.; Shojaei, F.; Zhuang, X. A novel two-dimensional C36 fullerene network; an isotropic, auxetic semiconductor with low thermal conductivity and remarkable stiffness. *Mater. Today Nano* **2023**, *21*, 100280. [CrossRef]
12. Hou, L.; Cui, X.; Guan, B.; Wang, S.; Li, R.; Liu, Y.; Zhu, D.; Zheng, J. Synthesis of a monolayer fullerene network. *Nature* **2022**, *606*, 507–510. [CrossRef] [PubMed]
13. Hu, Y.; Wu, C.; Pan, Q.; Jin, Y.; Lyu, R.; Martinez, V.; Huang, S.; Wu, J.; Wayment, L.J.; Clark, N.A.; et al. Synthesis of γ-graphyne using dynamic covalent chemistry. *Nat. Synth.* **2022**, *1*, 449–454. [CrossRef]

14. Tong, Z.; Pecchia, A.; Yam, C.; Dumitrică, T.; Frauenheim, T. Phononic Thermal Transport along Graphene Grain Boundaries: A Hidden Vulnerability. *Adv. Sci.* **2021**, *8*, e2101624. [CrossRef] [PubMed]

15. Tong, Z.; Pecchia, A.; Yam, C.; Dumitrică, T.; Frauenheim, T. Ultrahigh Electron Thermal Conductivity in T-Graphene, Biphenylene, and Net-Graphene. *Adv. Energy Mater.* **2022**, *12*, 2200657. [CrossRef]

16. Kang, F.; Sun, L.; Gao, W.; Sun, Q.; Xu, W. On-Surface Synthesis of a Carbon Nanoribbon Composed of 4–5–6–8-Membered Rings. *ACS Nano* **2023**, *17*, 8717–8722. [CrossRef]

17. Algara-Siller, G.; Severin, N.; Chong, S.Y.; Björkman, T.; Palgrave, R.G.; Laybourn, A.; Antonietti, M.; Khimyak, Y.Z.; Krasheninnikov, A.V.; Rabe, J.P.; et al. Triazine-based graphitic carbon nitride: A two-dimensional semiconductor. *Angew. Chem. Int. Ed.* **2014**, *53*, 7450–7455. [CrossRef]

18. Mahmood, J.; Lee, E.K.; Jung, M.; Shin, D.; Jeon, I.-Y.; Jung, S.-M.; Choi, H.-J.; Seo, J.-M.; Bae, S.-Y.; Sohn, S.-D.; et al. Nitrogenated holey two-dimensional structures. *Nat. Commun.* **2015**, *6*, 6486. [CrossRef]

19. Zeng, J.; Chen, Z.; Zhao, X.; Yu, W.; Wu, S.; Lu, J.; Loh, K.P.; Wu, J. From All-Triazine C_3N_3 Framework to Nitrogen-Doped Carbon Nanotubes: Efficient and Durable Trifunctional Electrocatalysts. *ACS Appl. Nano Mater.* **2019**, *2*, 7969–7977. [CrossRef]

20. Mahmood, J.; Lee, E.K.; Jung, M.; Shin, D.; Choi, H.-J.; Seo, J.-M.; Jung, S.-M.; Kim, D.; Li, F.; Lah, M.S.; et al. Two-dimensional polyaniline (C_3N) from carbonized organic single crystals in solid state. *Proc. Natl. Acad. Sci. USA* **2016**, *113*, 7414–7419. [CrossRef]

21. Kumar, P.; Vahidzadeh, E.; Thakur, U.K.; Kar, P.; Alam, K.M.; Goswami, A.; Mahdi, N.; Cui, K.; Bernard, G.M.; Michaelis, V.K.; et al. C_3N_5: A Low Bandgap Semiconductor Containing an Azo-Linked Carbon Nitride Framework for Photocatalytic, Photovoltaic and Adsorbent Applications. *J. Am. Chem. Soc.* **2019**, *141*, 5415–5436. [CrossRef] [PubMed]

22. Bahari, Y.; Mortazavi, B.; Rajabpour, A.; Zhuang, X.; Rabczuk, T. Application of two-dimensional materials as anodes for rechargeable metal-ion batteries: A comprehensive perspective from density functional theory simulations. *Energy Storage Mater.* **2020**, *35*, 203–282. [CrossRef]

23. Shi, Y.-B.; Lv, S.-H.; Shao, Z.-F.; Dong, H.-K.; Cao, S.; Qian, P. A first-principles study of 1D and 2D C_{60} nanostructures: Strain effects on band alignments and carrier mobility. *J. Physics Condens. Matter* **2023**, *35*, 225701. [CrossRef] [PubMed]

24. Shi, Y.-B.; Chen, Y.-Y.; Wang, H.; Cao, S.; Zhu, Y.-X.; Chu, M.-F.; Shao, Z.-F.; Dong, H.-K.; Qian, P. Investigation of the mechanical and transport properties of $InGeX_3$ (X = S, Se and Te) monolayers using density functional theory and machine learning. *Phys. Chem. Chem. Phys.* **2023**, *25*, 13864–13876. [CrossRef] [PubMed]

25. Izadifar, M.; Ukrainczyk, N.; Koenders, E. Silicate Dissolution Mechanism from Metakaolinite Using Density Functional Theory. *Nanomaterials* **2023**, *13*, 1196. [CrossRef]

26. Izadifar, M.; Valencia, N.C.; Xiao, P.; Ukrainczyk, N.; Koenders, E. 3D Off-Lattice Coarse-Grained Monte Carlo Simulations for Nucleation of Alkaline Aluminosilicate Gels. *Materials* **2023**, *16*, 1863. [CrossRef]

27. Aldakheel, F.; Satari, R.; Wriggers, P. Feed-Forward Neural Networks for Failure Mechanics Problems. *Appl. Sci.* **2021**, *11*, 6483. [CrossRef]

28. Aldakheel, F.; Kandekar, C.; Bensmann, B.; Dal, H.; Hanke-Rauschenbach, R. Electro-chemo-mechanical induced fracture modeling in proton exchange membrane water electrolysis for sustainable hydrogen production. *Comput. Methods Appl. Mech. Eng.* **2022**, *400*, 115580. [CrossRef]

29. Aldakheel, F.; Elsayed, E.S.; Zohdi, T.I.; Wriggers, P. Efficient multiscale modeling of heterogeneous materials using deep neural networks. *Comput. Mech.* **2023**, *72*, 155–171. [CrossRef]

30. Kresse, G.; Furthmüller, J. Efficient iterative schemes for *ab initio* total-energy calculations using a plane-wave basis set. *Phys. Rev. B* **1996**, *54*, 11169–11186. [CrossRef]

31. Perdew, J.P.; Burke, K.; Ernzerhof, M. Generalized Gradient Approximation Made Simple. *Phys. Rev. Lett.* **1996**, *77*, 3865–3868. [CrossRef]

32. Grimme, S.; Antony, J.; Ehrlich, S.; Krieg, H. A consistent and accurate ab initio parametrization of density functional dispersion correction (DFT-D) for the 94 elements H-Pu. *J. Chem. Phys.* **2010**, *132*, 154104. [CrossRef]

33. Monkhorst, H.J.; Pack, J.D. Special points for Brillouin-zone integrations. *Phys. Rev. B* **1976**, *13*, 5188–5192. [CrossRef]

34. Krukau, A.V.; Vydrov, O.A.; Izmaylov, A.F.; Scuseria, G.E. Influence of the exchange screening parameter on the performance of screened hybrid functionals. *J. Chem. Phys.* **2006**, *125*, 224106. [CrossRef]

35. Shishkin, M.; Kresse, G. Self-consistentGWcalculations for semiconductors and insulators. *Phys. Rev. B Condens. Matter Mater. Phys.* **2007**, *75*, 235102. [CrossRef]

36. Mortazavi, B.; Zhuang, X.; Rabczuk, T.; Shapeev, A.V. Atomistic Modeling of the Mechanical Properties: The Rise of Machine Learning Interatomic Potentials. *Mater. Horizons* **2023**, *10*, 1956–1968. [CrossRef] [PubMed]

37. Mortazavi, B.; Podryabinkin, E.V.; Roche, S.; Rabczuk, T.; Zhuang, X.; Shapeev, A.V. Machine-Learning Interatomic Potentials Enable First-Principles Multiscale Modeling of Lattice Thermal Conductivity in Graphene/Borophene Heterostructures. *Mater. Horizons* **2020**, *7*, 2359–2367. [CrossRef]

38. Ghorbani, K.; Mirchi, P.; Arabha, S.; Rajabpour, A.; Volz, S. Lattice Thermal Conductivity and Young's Modulus of XN4 (X = Be, Mg and Pt) 2D Materials Using Machine Learning Interatomic Potentials. *Phys. Chem. Chem. Phys.* **2023**, *25*, 12923–12933. [CrossRef]

39. Arabha, S.; Aghbolagh, Z.S.; Ghorbani, K.; Hatam-Lee, M.; Rajabpour, A. Recent Advances in Lattice Thermal Conductivity Calculation Using Machine-Learning Interatomic Potentials. *J. Appl. Phys.* **2021**, *130*, 210903. [CrossRef]
40. Mortazavi, B.; Silani, M.; Podryabinkin, E.V.; Rabczuk, T.; Zhuang, X.; Shapeev, A.V. First-Principles Multiscale Modeling of Mechanical Properties in Graphene/Borophene Heterostructures Empowered by Machine-Learning Interatomic Potentials. *Adv. Mater.* **2021**, *33*, 2102807. [CrossRef] [PubMed]